Polar positioning of a conjugation protein from the integrative and conjugative element ICE*Bs1* of *Bacillus subtilis*

Melanie B. Berkmen[1,2], Catherine A. Lee[1], Emma-Kate Loveday[2,3], and Alan D. Grossman[1]*

[1]Department of Biology; Massachusetts Institute of Technology; Cambridge, MA 02139

[2]Department of Chemistry and Biochemistry; Suffolk University; Boston, MA 02114

[3] Current address: Department of Microbiology and Immunology, 2350 Health Sciences Mall, University of British Columbia, Vancouver, BC Canada V6T 1Z4

running title: Polar ICE*Bs1* conjugation protein in *B. subtilis*

Key words: *Bacillus subtilis*, ICE*Bs1*, conjugative transposon, horizontal gene transfer, ATPase

* Correspondence to:
Alan D. Grossman
Department of Biology
Building 68-530
MIT
Cambridge, MA 02139
phone: 617-253-1515
fax: 617-253-2643
e-mail: adg@mit.edu

Abstract

ICE*Bs1* is an integrative and conjugative element found in the chromosome of *Bacillus subtilis*. ICE*Bs1* encodes functions needed for its excision and transfer to recipient cells. We found that the ICE*Bs1* gene *conE* (formerly *yddE*) is required for conjugation and that conjugative transfer of ICE*Bs1* requires a conserved ATPase domain of ConE. ConE belongs to the HerA/FtsK superfamily of ATPases, which includes the well-characterized proteins FtsK, SpoIIIE, VirB4, and VirD4. We found that a ConE-GFP (green fluorescent protein) fusion associated with the membrane predominantly at the cell poles in ICE*Bs1* donor cells. At least one ICE*Bs1* product likely interacts with ConE to target it to the membrane and cell poles, as ConE-GFP was dispersed throughout the cytoplasm in a strain lacking ICE*Bs1*. We also visualized the subcellular location of ICE*Bs1*. When integrated in the chromosome, ICE*Bs1* was located near midcell along the length of the cell, a position characteristic of that chromosomal region. Following excision, ICE*Bs1* was more frequently found near a cell pole. Excision of ICE*Bs1* also caused altered positioning of at least one component of the replisome. Taken together, our findings indicate that ConE is a critical component of the ICE*Bs1* conjugation machinery, that conjugative transfer of ICE*Bs1* from *B. subtilis* likely initiates at a donor cell pole, and that ICE*Bs1* affects the subcellular position of the replisome.

Introduction

Integrative and conjugative elements (also known as conjugative transposons) and conjugative plasmids are key elements in horizontal gene transfer and are capable of mediating their own transfer from donor to recipient cells. ICE*Bs1* is an integrative and conjugative element found in some *Bacillus subtilis* strains. Where found, ICE*Bs1* is integrated into the leucine tRNA gene *trnS-leu2* (Fig. 1) (7, 14, 21).

ICE*Bs1* gene expression, excision, and potential mating are induced by activation of RecA during the SOS response following DNA damage (7). In addition, ICE*Bs1* is induced by increased production or activation of the ICE*Bs1*-encoded regulatory protein RapI. Production and activity of RapI are indicative of the presence of potential mating partners that do not contain a copy of ICE*Bs1* (7). Under inducing conditions, the ICE*Bs1* repressor ImmR (6) is inactivated by proteolytic cleavage mediated by the anti-repressor and protease ImmA (12). Most ICE*Bs1* genes then become highly expressed (7). One of these genes (*xis*) encodes an excisionase, which in combination with the element's integrase causes efficient excision and formation of a double-stranded circle (7, 38). The circular form is nicked at the origin of transfer, *oriT*, by a DNA relaxase, the product of *nicK* (39). Under appropriate conditions, ICE*Bs1* can then mate into *B. subtilis* and other species, including the pathogens *Listeria monocytogenes* and *B. anthracis* (7). Once transferred to a recipient, ICE*Bs1* can be stably integrated into the genome at its attachment site in *trnS-leu2* by the ICE*Bs1*-encoded integrase (38).

In contrast to what is known about ICE*Bs1* genes and proteins involved in excision, integration, and gene regulation, less is known about the components that make up the Gram-positive mating machinery, defined as the conjugation proteins involved in DNA transfer (18, 24). The well-characterized Gram-negative mating machinery can serve as a preliminary model

(15, 16, 37, 48). The Gram-negative mating machinery is a Type IV secretion (T4S) system composed of at least eight conserved proteins that span the cell envelope. For example, the conjugation apparatus of the *Agrobacterium tumefaciens* Ti plasmid (pTi) is composed of 11 proteins (VirB1 through VirB11) including the ATPase VirB4 (16). VirB4 family members interact with several components of their cognate secretion systems and may energize machine assembly and/or substrate transfer (16, 48). The secretion substrate is targeted to the conjugation machinery by a "coupling protein". Coupling proteins, such as VirD4 of pTi, interact with a protein attached to the end of the DNA substrate and couple the substrate to other components of the conjugation machinery. Coupling proteins might also energize the translocation of DNA through the machinery. Both VirB4 and VirD4 belong to the large HerA/FtsK superfamily of ATPases (29). Two other characterized members of this superfamily are the chromosome partitioning proteins FtsK and SpoIIIE (29), which are ATP-dependent DNA pumps {reviewed in (2)}.

Some of the proteins encoded by Gram-positive conjugative elements are homologous to components of the conjugation machinery from Gram-negative organisms (1, 9, 14, 29) indicating that some aspects of conjugative DNA transfer may be similar in Gram-positives and Gram-negatives. For example, ConE (formerly YddE) of ICE*Bs1* has sequence similarities to VirB4 (29). YdcQ may be the ICE*Bs1*-encoded coupling protein as it is phylogenetically related to other coupling proteins (29, 44). Despite some similarities, the cell envelopes and many of the genes encoding the conjugation machinery are different between Gram-positive and Gram-negative organisms, indicating that there are likely to be significant structural and mechanistic differences as well.

To begin to define the conjugation machinery of ICE*Bs1* and to understand spatial aspects of

conjugation, we examined the function and subcellular location of ConE of ICE*Bs1*. Our results indicate that ConE is likely a crucial ATPase component of the ICE*Bs1* conjugation machinery. We found that ConE and excised ICE*Bs1* DNA were located at or near the cell poles. We propose that the conjugation machinery is likely located at the cell poles and that mating might occur from a donor cell pole.

Materials and Methods

Media and growth conditions

For *B. subtilis* and *E. coli* strains, routine growth and strain constructions were done on LB medium. For all reported experiments with *B. subtilis*, cells were grown at 37°C in S7 defined minimal medium (54) with MOPS buffer at 50 mM rather than 100 mM, with 0.1% glutamate and supplemented with auxotrophic requirements (40 µg/ml tryptophan; 40 µg/ml phenylalanine; 200 µg/ml threonine) as needed. Either 1% glucose or succinate was used as a carbon source, as indicated. Antibiotics were used at standard concentrations (27).

Strains, alleles, and plasmids

E. coli strains used for routine cloning were AG115 (MC1061 F'*lacI*^{q} *lacZ*::Tn*5*) and AG1111 (MC1061 F'*lacI*^{q} *lacZ*M15 Tn*10*). *B. subtilis* strains used in experiments and their relevant genotypes are listed in Table 1 and are derivatives of JH642 containing the *trpC2* and *pheA1* mutations (45). *B. subtilis* strains were constructed by natural transformation (27) or conjugation (7). Strains cured of ICE*Bs1* (ICE*Bs1*^{0}), the spontaneous streptomycin (*str*) resistant allele, Δ(*rapIphrI*)342::*kan*, and ICE*Bs1*::*kan* were described previously (7). The unmarked deletions Δ*nicK306* (39) and Δ*xis190* (38) and the tau-YFP (*dnaX-yfp*) fusion (42) have also been described. All cloned fragments into newly constructed plasmids were verified by

sequencing.

(i) Unmarked *conE* mutations. The basic strategy for constructing unmarked alleles of *conE* was similar to that previously described for construction of Δ*nicK306* (39). *conE*Δ(*88-808*) is an unmarked, in-frame deletion of codons 88 through 808 of *conE*, resulting in the fusion of codons 1 through 87 to codons 809 through 831. This deletion keeps the upstream and overlapping *yddD* gene intact. The splice-overlap-extension PCR method (28) was used to generate a 1.9 kb DNA fragment containing the *conE*Δ(*88-808*) allele. This fragment was cloned into the chloramphenicol resistance vector pEX44 (19)), upstream of *lacZ*. The resulting plasmid, pMMB941, was used to replace *conE* with *conE*Δ(*88-808*) in strain JMA168.

Mutations in the Walker A and B motifs of *conE* were made using a strategy similar to that for construction of *conE*Δ(*88-808*). *conE*(*K476E*) contains an unmarked missense mutation in *conE*, converting a lysine at codon 476 to a glutamic acid. *conE*(*D703A/E704A*) contains two missense mutations, converting the aspartate and glutamate at 703 and 704 in *conE* to alanines. DNA fragments (3 kb) containing the *conE* alleles were generated by PCR and cloned into pKG1 (7). The resulting plasmids, pMMB1083 and pMMB1231, were used to introduce *conE*(*K476E*) and *conE*(*D703A/E704A*), respectively, into the chromosome.

(ii) Constructs for complementation of *conE* alleles. The *thrC*::{(P*xis*-(*conE-lacZ*)) *mls*} allele was constructed to express *conE* from its presumed native promoter (P*xis*) of ICE*Bs1*. *conE* was cloned into pKG1, downstream of P*xis* and upstream of *lacZ*, creating plasmid pMMB943. pMMB943 was transformed into JH642 to create the *thrC*::{(P*xis*-(*conE-lacZ*)) *mls*} allele. A similar strategy was used to produce *thrC*::{(P*xis*-(*yddD conE-lacZ*)) *mls*} from plasmid pMMB942, *thrC*::{(P*xis*-(*yddD-lacZ*)) *mls*} from plasmid pMMB1004, and *thrC*::{(P*xis*-(*yddD conE*(*K476E*)*-lacZ*)) *mls*} from pMMB1083. *thrC325*::{(ICE*Bs1*-311 (Δ*attR*::*tet*)) *mls*} (strain

MMB1218) contains ICE*Bs1* inserted at *thrC*. It is incapable of excision due to deletion of the right-side attachment site *attR* as described previously (39).

(iii) Overexpression of RapI. *rapI* was overexpressed from P*spank*(*hy*) in single copy in the chromosome at *amyE* (*amyE*::{(P*spank*(*hy*)-*rapI*) *spc*}) as described (7), or from P*xyl*, also at *amyE*. To construct *amyE*::{(P*xyl-rapI*) *spc*}, *rapI* was cloned downstream of P*xyl* in vector pDR160, (from D. Rudner, Harvard Medical School, Boston). The resulting plasmid, pMMB856, was integrated at *amyE* in *B. subtilis* by homologous recombination.

(iv) Construction of a vector for double integration at *lacA*. We constructed the vector pMMB752 for introducing DNA via double crossover at *lacA*. First, an 891 bp PCR fragment of the 5' end of *lacA* was cloned into the tetracycline-resistance vector pDG1513 to generate pMMB739. Second, a 1042 bp PCR fragment of the 3' end of *lacA* was cloned into pMMB739 to generate pMMB752.

(v) GFP fusions to ConE, ConEΔ(88-808), and ConE(K476E). The vector pMMB759 was derived from pMMB752. It allows fusion of the C-terminus of a protein to a 23 amino acid linker followed by monomeric GFPmut2 (mGFPmut2). A fragment (containing the 23 amino acid linker and mGFPmut2) was digested from pLS31 (49) with *Xho*I and *Sph*I and ligated into pMMB752 to generate pMMB759.

lacA::{(P*xis-yddD conE-mgfpmut2*) *tet*} expresses *yddD* and *conE-mgfpmut2* from the presumed native promoter (P*xis*) of ICE*Bs1*. We inserted a 363 bp PCR fragment containing the P*xis* promoter into pMMB759, upstream of *mgfpmut2*, generating pMMB762. A 2.9 kb PCR fragment of *yddD* and *conE* missing its stop codon was cloned into the *Kpn*I and *Xho*I sites of pMMB762, downstream of P*xis* and upstream of *mgfpmut2*, creating plasmid pMMB786. pMMB786 was transformed into JH642 to create the *lacA*::{(P*xis-yddD conE-mgfpmut2*) *tet*}

allele. *lacA*::{(P*xis*-*yddD conE*Δ(*88-808*)-*mgfpmut2*) *tet*} and *lacA*::{(P*xis*-*yddD conE*(*K476E*)-*mgfpmut2*) *tet*} were generated using a similar strategy but using PCR fragments synthesized from templates pMMB1082 for *conE*Δ(*88-808*) and pMMB1083 for *conE*(*K476E*).

ConE-GFP was partially functional in mating. Expression of *yddD* and *conE-gfp* from their presumed native promoter (P*xis*) at the heterologous site (*lacA*) in *conE* (K476E) donors increased the frequency of mating at least 250-fold (0.001% mating efficiency for strain MMB1134 compared to <0.000004% for MMB1118). In addition, expression of *conE-gfp* at *lacA* in *conE*$^+$ donors had no effect on mating frequency (8% mating efficiency for strain MMB968 compared to 7% for JMA168).

(vi) Visualization of chromosomal regions using the *lac* operator/*lac* repressor system. The *lac* operator/*lac* repressor system has been used previously to visualize chromosome regions in *B. subtilis* (e.g., (42, 50, 56)). To mark the 47° (in ICE*Bs1*) and 48° (outside of ICE*Bs1*) regions, we inserted a plasmid containing a tandem array of *lac* operators near *yddM* (pMMB779) and *ydeDE* (pMMB854), respectively, by single crossover. *yddM* (47°) and *ydeDE* (48°) are not disrupted in these constructs. We inserted a 466 bp PCR fragment of the 3' end of *yddM* into the *Nhe*I and *Eco*RI sites of pPSL44a to generate pMMB779. pPSL44a is pGEMcat containing an *Xho*I fragment from pLAU43 that includes a 4.5 kb array of *lac* operators (11). Ten base pairs of random sequence intersperses each *lacO* site of pLAU43, leading to greater genetic stability by reducing the frequency of recombination (35). We inserted a 728 bp PCR fragment including the 3' ends and intergenic region between *ydeD* and *ydeE* into the *Nhe*I and *EcoR*I sites of pPSL44a to generate pMMB845. The *lac* operator arrays were amplified *in vivo* by selecting for resistance to chloramphenicol (25 µg/ml) as described previously (56).

Mating Assays

We assayed ICE*Bs1* DNA transfer as described previously (7). We used donor *B. subtilis* cells in which ICE*Bs1* contained a kanamycin resistance gene. Recipient cells lacked ICE*Bs1* (ICE*Bs1*^{0}) and were distinguishable from donors as they were streptomycin resistant. Donors and recipient cells were grown separately in minimal glucose medium for at least four generations. ICE*Bs1* was induced in the donors in mid-exponential phase (optical density at 600 nm to ~0.4) by addition of IPTG (1 mM) for 1 hr to induce expression of *rapI* (from P*spank*(*hy*)-*rapI*). Donors and ICE*Bs1*^{0} recipient cells (CAL419) were mixed and filtered on sterile cellulose nitrate membrane filters (0.2 μm pore size). Filters were placed in Petri dishes containing Spizizen's minimal salts (27) and 1.5% agar and incubated at 37ºC for 3 hours. Cells were washed off the filter and the number of transconjugants (recipients that received ICE*Bs1*) per ml was measured by determining the number of kan^R strep^R colony forming units (CFUs) after the mating. Percent mating is the (number of transconjugant CFUs per donor CFU) x 100%.

Live cell fluorescence microscopy

Microscopy was performed as described (10). Cells were grown at least four generations to mid-exponential phase (optical density at 600 nm to ~0.4) in minimal medium. RapI overexpression was induced with either 1 mM IPTG for 1 hour for strains containing *amyE*::{(P*spank*(*hy*)-*rapI*) *spc*} or with 1% xylose for ~2 hours for strains containing *amyE*::{(P*xyl*-*rapI*) *spc*}. Cells were stained with FM4-64 (1 μg/ml; Molecular Probes) to visualize membranes. Live cells were immobilized on pads of 1% agarose containing Spizizen's minimal salts. All images were captured at room temperature with a Nikon E800 microscope equipped with a 100x DIC objective and a Hamamatsu digital camera. We used the Chroma filter sets 41002b (TRITC) for FM4-64, 31044 for CFP, 41012 for GFP, and 41028 for YFP.

Improvision Openlabs 4.0 Software was used to process images. Cell length and focus position was measured and plotted as described previously (10, 40). Each strain was examined in at least two independent experiments with similar results.

Results

conE is required for mating

Conjugative transfer of ICE*Bs1* is a multi-step process. Previous work indicated that *conE* is not required for ICE*Bs1* gene expression, excision, integration, circularization, or nicking (6, 7, 12, 38, 39). Since ConE is a putative ATPase and distantly related to other ATPases known to be required for conjugation, we tested the effects of *conE* mutations on mating of ICE*Bs1*.

We constructed three different *conE* alleles: 1) an in-frame deletion {*conE*Δ(*88-808*)} removing codons 88 through 808 (of 831); 2) a missense mutation in the Walker A box {*conE*(*K476E*)} that is predicted to eliminate nucleotide binding; and 3) a double missense mutation in the Walker B box {*conE*(*D703A/E704A*)} that is predicted to eliminate ATPase activity {reviewed in (26)}. Each *conE* mutant allele was introduced unmarked into ICE*Bs1* replacing the wild type allele (see Materials and Methods).

We found that *conE* is required for ICE*Bs1* conjugative transfer. We compared mating efficiencies of ICE*Bs1* from donor strains containing the various *conE* alleles into recipient *B. subtilis* cells lacking ICE*Bs1* (Fig. 2). ICE*Bs1* was induced by overproduction of RapI from a heterologous promoter and potential donor cells were mixed with potential recipients that lacked ICE*Bs1*, essentially as described (7). The donor ICE*Bs1* contained an antibiotic resistance marker that had been inserted to allow selection and monitoring of ICE*Bs1* acquisition (7). A donor strain with an intact *conE* (*conE*$^{+}$) transferred ICE*Bs1* with an average mating frequency

of ~7% {percent transconjugant colony forming units (CFU) per donor CFU; Fig. 2a}. In contrast, there were no detectable transconjugants from the ICE*Bs1 conE* mutants (Fig. 2b-d).

Consistent with previous results indicating that *conE* is not involved in ICE*Bs1* gene expression, excision, or circularization (6, 7, 12, 38, 39), we found that neither *conE*(*K476E*) nor *conE*Δ(*88-808*) mutant alleles had any detectable effect on these processes (data not shown).

Complementation tests with *conE*

We used complementation tests to determine if the defect in mating caused by the *conE*(*K476E*) mutation was due to loss of ConE function and/or an unintended effect on some other gene. The defect in mating caused by the *conE*(*K476E*) mutation was complemented partially when wild type *conE* was provided in the donor in *trans* under control of the ICE*Bs1* promoter P*xis* (Fig. 2e). Measurements of mRNA levels using DNA microarrays indicated that the partial complementation is not due to unexpected defects in expression of other ICE*Bs1* genes or of P*xis-conE* (data not shown).

The partial complementation of the *conE*(*K476E*) mutation is probably due, in part, to inefficient translation of wild type ConE expressed from P*xis-conE*. *yddD*, the gene immediately upstream of *conE*, is predicted to overlap with the first 37 codons of *conE*, and thus the two are likely to be translationally coupled. Complementation of the *conE*(*K476E*) mutant was significantly increased when *yddD* and *conE* were expressed together (P*xis-yddD conE*) than when *conE* was expressed alone (P*xis-conE*) (Fig. 2e, f). Neither expression of *yddD* alone nor expression of *yddD* and *conE*(*K476E*) together improved the efficiency of transfer of the ICE*Bs1 conE* mutant (Fig. 2g, h). *conE*(*K476E*) was complemented fully if an additional copy of ICE*Bs1* was placed at the ectopic locus *thrC* (Fig. 2i). These results and results from additional mating experiments with *conE* expressed in recipients indicate that *conE* function is needed in

the donor and not the recipient (data not shown). Based on these findings, we suspect that ConE is not efficiently translated and assembled into an active complex when expressed in trans to YddD and other ICE*Bs1* proteins.

Taken together, our results indicate that ConE and its ATPase domain are required in the donor for mating of ICE*Bs1*, but are not required for induction of ICE*Bs1*, excision, circularization, nicking, or integration. Based on these results and the homology of ConE to VirB4-like conjugative ATPases, the simplest interpretation is that ConE is a component of the ICE*Bs1* conjugation machinery and that ATP binding and hydrolysis are required for ConE function in ICE*Bs1* DNA transfer.

ConE-GFP localizes to the cell poles, in close association with the membrane

We found that ConE is located predominantly at the cell poles, in close association with the membrane. We visualized the subcellular location of ConE in live cells by visualizing a fusion of GFP to the C-terminus of ConE. *conE-gfp* was expressed from its presumed native promoter (P*xis*), together with *yddD*, at the heterologous locus (*lacA*) outside of ICE*Bs1*. This fusion was partially functional and did not interfere with transfer of *conE*$^{+}$ ICE*Bs1* (see Materials and Methods). Most experiments using ConE-GFP were done with strains that also contained a wild-type version of *conE* in ICE*Bs1*.

We monitored ConE-GFP prior to and after induction of ICE*Bs1* gene expression. Little or no fluorescence was observed in cells in which ICE*Bs1* gene expression was not induced (data not shown). This was expected since the P*xis* promoter driving expression of *conE-gfp* is not active without induction (6, 7, 12). When ICE*Bs1* gene expression was induced by overproduction of RapI, ConE-GFP was found predominantly at the cell poles in most cells (Fig. 3A). This is most evident with simultaneous visualization of ConE-GFP and the cell membrane

stained with the dye FM4-64 (Fig. 3B). ConE-GFP appeared to form a "polar cap" along the entire pole near the membrane. ConE-GFP was most often found at both cell poles, but was also commonly observed at only one pole. A lower level of fluorescence was also detected throughout the cell and sometimes along the lateral sides of the cells.

Positioning of ConE-GFP at the cell poles requires at least one other ICE*Bs1* gene

The polar positioning of ConE-GFP did not depend on the wild type *conE* in ICE*Bs1*. We visualized ConE-GFP in cells deleted for *conE* {*conE*Δ(*88-808*)} at its native locus in ICE*Bs1* and found that its subcellular position was indistinguishable from that in cells expressing wild type *conE* (Fig. 3C). These results indicate that the positioning of ConE-GFP at the poles does not depend on expression of wild-type *conE* in ICE*Bs1*. In addition, we fused *conE*Δ(*88-808*) to *gfp* and expressed this from P*xis* (along with *yddD*) as above. The ConEΔ(88-808)-GFP fusion was found throughout the cyptoplasm, both in the presence and absence of functional *conE* in ICE*Bs1* (Fig 3D; data not shown). These results indicate that ConEΔ(88-808)-GFP is not capable of localizing at the cell poles.

We found that positioning of ConE-GFP to the membrane and cell poles required at least one other ICE*Bs1* gene. In cells missing ICE*Bs1* entirely (ICE*Bs1*^{0}), ConE-GFP was dispersed throughout the cytoplasm (Fig. 3E). In these experiments, ConE-GFP was produced constitutively from P*xis* in combination with YddD (P*xis-yddD conE-gfp*). These results indicate that proper positioning of ConE-GFP at the poles and near the membrane requires an ICE*Bs1* gene product and that YddD is not sufficient to recruit ConE-GFP to the membrane. Alternatively, positioning of ConE-GFP could require interaction with ICE*Bs1* DNA, although we think this is less likely.

296 The positioning of ConE-GFP near the cell membrane is consistent with a prior report that
297 identified ConE (YddE) as one of many proteins found in sub-membrane fractions of *B. subtilis*
298 (13). However, ConE does not contain any predicted transmembrane segments according to
299 several transmembrane and subcellular localization prediction programs, including Phobius (31),
300 Polyphobius (32), HHMTOP (52, 53), TopPred (17), cPsortdb (46), DAS (20), and PHDhtm
301 (47). Several other ICE*Bs1* proteins {products of *ydcQ*, *yddB*, *yddC*, *yddD*, *yddG*, *cwlT*
302 (formerly *yddH*), *yddI*, *yddJ*,and *yddM*} contain one or more predicted transmembrane segments
303 (Fig. 1). We do not yet know which, if any, of these proteins are involved in membrane
304 association of ConE, but we favor a model in which at least one of these ICE*Bs1* proteins
305 interacts with ConE and targets it to the polar membrane.

306 **Positioning of ConE-GFP at the cell poles does not require a functional *conE***

307 We found that positioning of ConE at the poles did not require that ConE be functional for
308 mating. We fused the mating-deficient allele *conE*(*K476E*) to *gfp* and expressed this fusion from
309 P*xis* (along with *yddD*) as above. Following induction of ICE*Bs1*, ConE(K476E)-GFP was
310 found at the cell poles near the membrane (Fig. 3F) similar to the location of wild-type ConE-
311 GFP (Fig. 3A, B). This polar localization of ConE(K476E)-GFP did not depend on a functional
312 copy of *conE* in ICE*Bs1* (data not shown). Since ConE(K476E) localized properly but did not
313 support mating, these results indicate that positioning of ConE at the cell poles is not sufficient
314 for its function in mating. Furthermore, assuming that the ConE(K476E) mutant protein is
315 defective in nucleotide binding, as predicted, these results indicate that neither binding nor
316 hydrolysis of ATP by ConE is required for its proper subcellular positioning.

Following induction, ICE*Bs1* DNA is found more frequently at the cell poles

We determined the subcellular location of ICE*Bs1* DNA in live cells and compared this with the location of nearby chromosomal DNA (Fig. 4). These comparisons were done in cells with ICE*Bs1* integrated in the genome in its normal attachment site at 47° and in cells in which ICE*Bs1* was induced to excise (through overproduction of RapI). We inserted an array of *lac* operators (*lacO*) in the right end of ICE*Bs1*, adjacent to *yddM* (47°), or outside of ICE*Bs1*, adjacent to *ydeD*, at 48° in the chromosome (Materials and Methods). We visualized the location of the *lacO* array using a fusion of Lac repressor to the cyan fluorescent protein (LacI-CFP). The position of LacI-CFP is indicative of the subcellular position of either double stranded ICE*Bs1* DNA or chromosomal DNA, depending on the location of the *lacO* array.

We examined cells growing slowly, when most cells were generally engaged in no more than one round of replication. Under these conditions, most cells contain one incompletely replicated chromosome, and therefore contain one or two copies of each chromosomal region. Without induction, ICE*Bs1* DNA is integrated into the chromosome near 47° (7, 38). As expected, we found that most uninduced cells (88% of 1535 cells) contained one or two foci of double-stranded ICE*Bs1* DNA (Fig. 4A). In cells with a single focus, the ICE*Bs1* DNA was generally located near midcell (Fig. 4A). Approximately 94% of these cells (of 246 cells with a single focus) had the focus in the middle 50% of cell length. Only 6% of cells (of 246) had the focus of ICE*Bs1* DNA in a polar quarter of the cell. These findings are consistent with expectations for this region of the chromosome based on previously published findings (11, 40, 50, 56).

In contrast to the position of ICE*Bs1* when integrated in the chromosome, significantly more cells had a focus of ICE*Bs1* DNA in a polar quarter after induction and excision. Overproduction of RapI causes efficient induction of ICE*Bs1* gene expression, excision from the chromosome,

and formation of a double stranded circle (7, 38, 39). Under these conditions, most cells (87% of 1804 cells) contained one or two foci of double-stranded ICE*Bs1* DNA (Fig. 4B), similar to that in uninduced cells (Fig. 4A). However, following induction, 41% of cells (of 489) with a single focus of ICE*Bs1* DNA had the focus in a polar quarter, an ~7-fold increase compared to that in uninduced cells (6%). These results indicate that ICE*Bs1* DNA is found more frequently near a cell pole following excision than when integrated in the chromosome.

The subcellular position of the 48° region of the chromosome, near the ICE*Bs1* attachment site, changed little, if at all, following induction of ICE*Bs1* gene expression and excision. Following induction of ICE*Bs1* (by overproduction of RapI), only 10% of cells with a single focus of the 48° region (of 195 cells) had the focus in a polar quarter of the cell (Fig. 4C), compared with 41% of cells with a polar focus of ICE*Bs1* DNA (Fig. 4B). These results indicate that after excision, ICE*Bs1* DNA is found more frequently near the cell poles than the previously adjacent chromosomal region. Thus, the change in location of ICE*Bs1* DNA upon induction is specific to ICE*Bs1* and not the region of the chromosome where it normally resides. In cells in which ICE*Bs1* was not induced, the subcellular location of the 48° region of the chromosome was indistinguishable from that of integrated ICE*Bs1* DNA (at 47°), as expected. Only 6% of cells with a single focus had the focus in a polar quarter of the cell (data not shown).

Polar positioning of ICE*Bs1* following induction depends on excision

We found that excision of ICE*Bs1* from the chromosome was required for the increase in ICE*Bs1* foci that were in the polar quarters of the cell. We induced ICE*Bs1* gene expression in an *xis* null mutant incapable of excision. ICE*Bs1* gene expression is induced normally in excision-defective mutants (J. Auchtung, CAL, ADG, unpublished results). After induction of ICE*Bs1* gene expression in the *xis* mutant, we found that only 13% of cells (of 276 cells) with a

single focus of ICE*Bs1* had the focus in a polar quarter (Fig. 4D). This is in contrast to the 41% of *xis*$^+$ cells with ICE*Bs1* in a polar quarter (Fig. 4B). Thus, the change in position of ICE*Bs1* DNA upon induction likely requires its excision from the chromosome. This result is consistent with either ICE*Bs1* DNA appearing at the poles due to direct association with the conjugation machinery or due to its random positioning in the cell once it is released from the chromosome.

In contrast to the requirement for *xis* for the high frequency of ICE*Bs1* DNA found near the cell poles, *xis* was not required for polar positioning of ConE-GFP. Following induction of ICE*Bs1* carrying a *xis* deletion, ConE-GFP localization was indistinguishable from that of *xis*$^+$ ICE*Bs1* (Fig. 3G). Together, these results indicate that excisionase is required for the change in position of ICE*Bs1* DNA upon induction and that polar positioning of ConE-GFP is most likely not due to association with ICE*Bs1* DNA at the poles.

The position of the replication machinery is altered following induction of ICE*Bs1*

Excision of ICE*Bs1* generates an extrachromosomal circle, analogous to a circular plasmid. Previous work indicated that the subcellular position of replisome proteins was altered in cells containing a multi-copy plasmid (55). We therefore wished to determine if excision of ICE*Bs1* caused altered subcelluar positioning of the replisome. We visualized the location of one component of the replication machinery using a functional fusion of the Tau subunit of DNA polymerase to yellow fluorescent protein (YFP) (42). Components of the replisome (the complex of replication proteins associated with a replication fork) normally form discrete foci at regular positions (41, 43). During slow growth when most cells are engaged in no more than one round of replication at a time, most cells have one focus or two closely spaced foci of the replisome located near midcell along the length of the rod-shaped cell (10, 41).

Consistent with previous results, we found that during slow growth, only a small fraction of cells with ICE*Bs1* integrated in the chromosome (uninduced) had a focus of Tau-YFP in a polar quarter. Of 250 cells with a single focus of Tau-YFP, only 4% had the focus in a polar quarter (Fig. 4E). In contrast, following excision of ICE*Bs1*, induced by overproduction of RapI, the replication machinery was much more frequently observed in the polar quarters. Of 212 cells observed with a single focus of Tau-YFP, 32% had the focus in a polar quarter (Fig. 4F). We suspect that the replisome foci were associated with ICE*Bs1* DNA, although we have not been able to test this directly. Due to photo-bleaching, we were unable to capture high quality micrographs of both Tau-YFP and ICE*Bs1* DNA (LacI-CFP) foci in the same cells to determine if the foci co-localize. Nonetheless, our data indicate that the subcellular position of at least one component of the replication machinery is altered following induction of ICE*Bs1*. These results might indicate that ICE*Bs1* DNA is replicated autonomously after excision. We are currently investigating this possibility.

Discussion

We found that ConE (formerly YddE) and its ATPase motifs are required for conjugation of the integrative and conjugative element ICE*Bs1* of *B. subtilis*. We found that a ConE-GFP fusion was positioned predominantly at the cell poles, apparently associated with the membrane, and that this positioning required at least one other ICE*Bs1* gene product. In addition, after excision from the chromosome, ICE*Bs1* DNA was found more frequently near the cell poles. Our results indicate that ConE is most likely part of the ICE*Bs1* conjugation machinery. If its subcellular location is indicative of where the protein is functioning, then mating of ICE*Bs1* from *B. subtilis* likely occurs from a donor cell pole. Attempts to test this by directly visualizing mating pairs have so far been unsuccessful.

VirB4-like proteins

ConE belongs to the VirB4 clade of the HerA/FtsK superfamily of ATPases (29). Characterized members of this clade are required for substrate secretion, form membrane-associated oligomers, and interact with several components of their cognate secretion machineries (16, 48). Analysis of *virB4* Walker A box mutants indicates that ATP binding and/or hydrolysis is required for DNA transfer through the secretion machinery but not for association of VirB4 with itself or other machinery components (4, 57).

Results with the few Gram-positive VirB4 homologs that have been studied indicate that these proteins likely operate analogously to *A. tumefaciens* VirB4. The VirB4-like TcpF protein of the *Clostridium perfringens* plasmid pCW3 is required for DNA transfer and localizes to the cell poles (9, 51). Another VirB4-homolog, $Orf5_{pIP501}$ of the broad host-range plasmid pIP50, interacts with itself and several putative components of its cognate conjugation machinery (1).

Subcellular location of conjugation proteins

ConE-GFP appears associated with the cell membrane and predominantly at both cell poles, indicating that mating may occur at either end of a *B. subtilis* donor cell. Mating pairs of live *E. coli* cells have been observed using fluorescence microscopy (8, 36). Transfer of the conjugative plasmid R751 in *E. coli* can occur along any orientation between donors and recipients that are in direct contact, suggesting that the conjugative machinery of R751 may assemble along both the lateral and polar sides of the cell (36). This type of lateral and polar localization of the mating machinery has been directly observed for the R27 conjugative plasmid in *E. coli* (22, 25). R27's VirB4-like TrhC and coupling protein TraG were distributed at multiple sites along all sides of the cell.

In other systems, the mating machinery is seen at one or both cell poles. For example, the conjugative pore of the Gram-positive *Clostridium perfringens* plasmid pCW3, likely localizes at both cell poles as evidenced by immunofluorescence microscopy of the VirB4-like TcpF protein (51). Components of the Gram-negative *Agrobacterium* pTi conjugative apparatus are typically located at a single cell pole (3, 5, 30, 33, 34).

For ConE, our results indicate that ATP-binding and hydrolysis are not required for targeting but at least one other ICE*Bs1* gene is required. The R27 VirB4-like protein TrhC also does not require a functional ATPase domain for localization but requires 12 of the other 18 R27 transfer proteins (23). VirB4 also does not require a functional ATPase domain for localization, but unlike TrhC or ConE, is able to target itself independently of other conjugation proteins (30).

It is not yet known where other ICE*Bs1* conjugation proteins are positioned in the cell or how they interact. Recent studies indicate that the Gram-positive conjugation apparatus may be as structurally complex as its Gram-negative counterpart (1, 9, 51). Since many ICE*Bs1* genes are

444 conserved between diverse conjugative elements found in a wide range of Gram-positive
445 bacteria, we suspect that an understanding of ICE*Bs1* will likely shed light on other conjugative
446 systems as well.
447
448 **Acknowledgements**
449 We are grateful to J.M. Auchtung for generous advice, strains, and protocols. This work was
450 supported primarily by Public Health Service grant GM50895 (ADG) and in part, by Suffolk
451 University Department of Chemistry and Biochemistry and a Suffolk University Summer
452 Stipend Award (MBB).
453

References

1. **Abajy, M. Y., J. Kopec, K. Schiwon, M. Burzynski, M. Doring, C. Bohn, and E. Grohmann.** 2007. A type IV-secretion-like system is required for conjugative DNA transport of broad-host-range plasmid pIP501 in gram-positive bacteria. J Bacteriol **189:**2487-2496.
2. **Allemand, J. F., and B. Maier.** 2009. Bacterial translocation motors investigated by single molecule techniques. FEMS Microbiol Rev **33:**593-610.
3. **Atmakuri, K., E. Cascales, O. T. Burton, L. M. Banta, and P. J. Christie.** 2007. *Agrobacterium* ParA/MinD-like VirC1 spatially coordinates early conjugative DNA transfer reactions. EMBO J **26:**2540-2551.
4. **Atmakuri, K., E. Cascales, and P. J. Christie.** 2004. Energetic components VirD4, VirB11 and VirB4 mediate early DNA transfer reactions required for bacterial type IV secretion. Mol Microbiol **54:**1199-1211.
5. **Atmakuri, K., Z. Ding, and P. J. Christie.** 2003. VirE2, a type IV secretion substrate, interacts with the VirD4 transfer protein at cell poles of *Agrobacterium tumefaciens*. Mol Microbiol **49:**1699-1713.
6. **Auchtung, J. M., C. A. Lee, K. L. Garrison, and A. D. Grossman.** 2007. Identification and characterization of the immunity repressor (ImmR) that controls the mobile genetic element ICE*Bs1* of *Bacillus subtilis*. Mol Microbiol **64:**1515-1528.
7. **Auchtung, J. M., C. A. Lee, R. E. Monson, A. P. Lehman, and A. D. Grossman.** 2005. Regulation of a *Bacillus subtilis* mobile genetic element by intercellular signaling and the global DNA damage response. Proc Natl Acad Sci U S A **102:**12554-12559.
8. **Babic, A., A. B. Lindner, M. Vulic, E. J. Stewart, and M. Radman.** 2008. Direct visualization of horizontal gene transfer. Science **319:**1533-1536.
9. **Bannam, T. L., W. L. Teng, D. Bulach, D. Lyras, and J. I. Rood.** 2006. Functional identification of conjugation and replication regions of the tetracycline resistance plasmid pCW3 from *Clostridium perfringens*. J Bacteriol **188:**4942-4951.
10. **Berkmen, M. B., and A. D. Grossman.** 2006. Spatial and temporal organization of the *Bacillus subtilis* replication cycle. Mol Microbiol **62:**57-71.
11. **Berkmen, M. B., and A. D. Grossman.** 2007. Subcellular positioning of the origin region of the *Bacillus subtilis* chromosome is independent of sequences within *oriC*, the site of replication initiation, and the replication initiator DnaA. Mol Microbiol **63:**150-165.
12. **Bose, B., J. M. Auchtung, C. A. Lee, and A. D. Grossman.** 2008. A conserved anti-repressor controls horizontal gene transfer by proteolysis. Mol Microbiol **70:**570-582.
13. **Bunai, K., M. Nozaki, M. Hamano, S. Ogane, T. Inoue, T. Nemoto, H. Nakanishi, and K. Yamane.** 2003. Proteomic analysis of acrylamide gel separated proteins immobilized on polyvinylidene difluoride membranes following proteolytic digestion in the presence of 80% acetonitrile. Proteomics **3:**1738-1749.
14. **Burrus, V., G. Pavlovic, B. Decaris, and G. Guedon.** 2002. The ICE*St1* element of *Streptococcus thermophilus* belongs to a large family of integrative and conjugative elements that exchange modules and change their specificity of integration. Plasmid **48:**77-97.
15. **Cascales, E., and P. J. Christie.** 2003. The versatile bacterial type IV secretion systems. Nat Rev Microbiol **1:**137-149.

16. **Christie, P. J., K. Atmakuri, V. Krishnamoorthy, S. Jakubowski, and E. Cascales.** 2005. Biogenesis, architecture, and function of bacterial type IV secretion systems. Annu Rev Microbiol **59:**451-485.
17. **Claros, M. G., and G. Von Heijne.** 1994. TopPred II: an improved software for membrane protein structure predictions. Comput Appl Biosci **10:**685-686.
18. **Clewell, D. B., and M. V. Francia.** 2004. Conjugation in Gram-positive bacteria., p. 227-260. *In* B. Funnell and G. Phillips (ed.), The Biology of Plasmids. ASM Press, Washington, D.C.
19. **Comella, N., and A. D. Grossman.** 2005. Conservation of genes and processes controlled by the quorum response in bacteria: characterization of genes controlled by the quorum-sensing transcription factor ComA in *Bacillus subtilis*. Mol Microbiol **57:**1159-1174.
20. **Cserzo, M., E. Wallin, I. Simon, G. Von Heijne, and A. Elofsson.** 1997. Prediction of transmembrane alpha-helices in prokaryotic membrane proteins: the dense alignment surface method. Protein Eng **10:**673-676.
21. **Earl, A. M., R. Losick, and R. Kolter.** 2007. *Bacillus subtilis* genome diversity. J Bacteriol **189:**1163-1170.
22. **Gilmour, M. W., T. D. Lawley, M. M. Rooker, P. J. Newnham, and D. E. Taylor.** 2001. Cellular location and temperature-dependent assembly of IncHI1 plasmid R27-encoded TrhC-associated conjugative transfer protein complexes. Mol Microbiol **42:**705-715.
23. **Gilmour, M. W., and D. E. Taylor.** 2004. A subassembly of R27-encoded transfer proteins is dependent on TrhC nucleoside triphosphate-binding motifs for function but not formation. J Bacteriol **186:**1606-1613.
24. **Grohmann, E., G. Muth, and M. Espinosa.** 2003. Conjugative plasmid transfer in gram-positive bacteria. Microbiol Mol Biol Rev **67:**277-301.
25. **Gunton, J. E., M. W. Gilmour, G. Alonso, and D. E. Taylor.** 2005. Subcellular localization and functional domains of the coupling protein, TraG, from IncHI1 plasmid R27. Microbiology **151:**3549-3561.
26. **Hanson, P. I., and S. W. Whiteheart.** 2005. AAA+ proteins: have engine, will work. Nat Rev Mol Cell Biol **6:**519-529.
27. **Harwood, C. R., and S. M. Cutting.** 1990. Molecular Biological Methods for *Bacillus*. John Wiley & Sons, Chichester.
28. **Horton, R. M., H. D. Hunt, S. N. Ho, J. K. Pullen, and L. R. Pease.** 1989. Engineering hybrid genes without the use of restriction enzymes: gene splicing by overlap extension. Gene **77:**61-68.
29. **Iyer, L. M., K. S. Makarova, E. V. Koonin, and L. Aravind.** 2004. Comparative genomics of the FtsK-HerA superfamily of pumping ATPases: implications for the origins of chromosome segregation, cell division and viral capsid packaging. Nucleic Acids Res **32:**5260-5279.
30. **Judd, P. K., R. B. Kumar, and A. Das.** 2005. Spatial location and requirements for the assembly of the *Agrobacterium tumefaciens* type IV secretion apparatus. Proc Natl Acad Sci U S A **102:**11498-11503.
31. **Kall, L., A. Krogh, and E. L. Sonnhammer.** 2004. A combined transmembrane topology and signal peptide prediction method. J Mol Biol **338:**1027-1036.
32. **Kall, L., A. Krogh, and E. L. Sonnhammer.** 2005. An HMM posterior decoder for sequence feature prediction that includes homology information. Bioinformatics **21 Suppl 1:**i251-257.

543 33. **Kumar, R. B., and A. Das.** 2002. Polar location and functional domains of the
544 *Agrobacterium tumefaciens* DNA transfer protein VirD4. Mol Microbiol **43:**1523-1532.
545 34. **Lai, E. M., O. Chesnokova, L. M. Banta, and C. I. Kado.** 2000. Genetic and
546 environmental factors affecting T-pilin export and T-pilus biogenesis in relation to
547 flagellation of *Agrobacterium* tumefaciens. J Bacteriol **182:**3705-3716.
548 35. **Lau, I. F., S. R. Filipe, B. Soballe, O. A. Okstad, F. X. Barre, and D. J. Sherratt.** 2003.
549 Spatial and temporal organization of replicating *Escherichia coli* chromosomes. Mol
550 Microbiol **49:**731-743.
551 36. **Lawley, T. D., G. S. Gordon, A. Wright, and D. E. Taylor.** 2002. Bacterial conjugative
552 transfer: visualization of successful mating pairs and plasmid establishment in live
553 *Escherichia coli*. Mol Microbiol **44:**947-956.
554 37. **Lawley, T. D., W. A. Klimke, M. J. Gubbins, and L. S. Frost.** 2003. F factor conjugation
555 is a true type IV secretion system. FEMS Microbiol Lett **224:**1-15.
556 38. **Lee, C. A., J. M. Auchtung, R. E. Monson, and A. D. Grossman.** 2007. Identification and
557 characterization of *int* (integrase), *xis* (excisionase) and chromosomal attachment sites of the
558 integrative and conjugative element ICE*Bs1* of *Bacillus subtilis*. Mol Microbiol **66:**1356-
559 1369.
560 39. **Lee, C. A., and A. D. Grossman.** 2007. Identification of the origin of transfer (*oriT*) and
561 DNA relaxase required for conjugation of the integrative and conjugative element ICE*Bs1* of
562 *Bacillus subtilis*. J Bacteriol **189:**7254-7261.
563 40. **Lee, P. S., D. C. Lin, S. Moriya, and A. D. Grossman.** 2003. Effects of the chromosome
564 partitioning protein Spo0J (ParB) on *oriC* positioning and replication initiation in *Bacillus*
565 *subtilis*. J Bacteriol **185:**1326-1337.
566 41. **Lemon, K. P., and A. D. Grossman.** 1998. Localization of bacterial DNA polymerase:
567 evidence for a factory model of replication. Science **282:**1516-1519.
568 42. **Lemon, K. P., and A. D. Grossman.** 2000. Movement of replicating DNA through a
569 stationary replisome. Mol Cell **6:**1321-1330.
570 43. **Meile, J. C., L. J. Wu, S. D. Ehrlich, J. Errington, and P. Noirot.** 2006. Systematic
571 localisation of proteins fused to the green fluorescent protein in *Bacillus subtilis*:
572 identification of new proteins at the DNA replication factory. Proteomics **6:**2135-2146.
573 44. **Parsons, J. A., T. L. Bannam, R. J. Devenish, and J. I. Rood.** 2007. TcpA, an
574 FtsK/SpoIIIE homolog, is essential for transfer of the conjugative plasmid pCW3 in
575 *Clostridium perfringens*. J Bacteriol **189:**7782-7790.
576 45. **Perego, M., G. B. Spiegelman, and J. A. Hoch.** 1988. Structure of the gene for the
577 transition state regulator, *abrB*: regulator synthesis is controlled by the *spo0A* sporulation
578 gene in *Bacillus subtilis*. Mol Microbiol **2:**689-699.
579 46. **Rey, S., M. Acab, J. L. Gardy, M. R. Laird, K. Defays, C. Lambert, and F. S.**
580 **Brinkman.** 2005. PSORTdb: a protein subcellular localization database for bacteria. Nucleic
581 Acids Res **33:**D164-168.
582 47. **Rost, B., P. Fariselli, and R. Casadio.** 1996. Topology prediction for helical transmembrane
583 proteins at 86% accuracy. Protein Sci **5:**1704-1718.
584 48. **Schroder, G., and E. Lanka.** 2005. The mating pair formation system of conjugative
585 plasmids-A versatile secretion machinery for transfer of proteins and DNA. Plasmid **54:**1-25.
586 49. **Simmons, L. A., B. W. Davies, A. D. Grossman, and G. C. Walker.** 2008. Beta clamp
587 directs localization of mismatch repair in *Bacillus subtilis*. Mol Cell **29:**291-301.

50. **Teleman, A. A., P. L. Graumann, D. C. Lin, A. D. Grossman, and R. Losick.** 1998. Chromosome arrangement within a bacterium. Curr Biol **8:**1102-1109.
51. **Teng, W. L., T. L. Bannam, J. A. Parsons, and J. I. Rood.** 2008. Functional characterization and localization of the TcpH conjugation protein from *Clostridium perfringens*. J Bacteriol **190:**5075-5086.
52. **Tusnady, G. E., and I. Simon.** 1998. Principles governing amino acid composition of integral membrane proteins: application to topology prediction. J Mol Biol **283:**489-506.
53. **Tusnady, G. E., and I. Simon.** 2001. The HMMTOP transmembrane topology prediction server. Bioinformatics **17:**849-850.
54. **Vasantha, N., and E. Freese.** 1980. Enzyme changes during *Bacillus subtilis* sporulation caused by deprivation of guanine nucleotides. J Bacteriol **144:**1119-1125.
55. **Wang, J. D., M. E. Rokop, M. M. Barker, N. R. Hanson, and A. D. Grossman.** 2004. Multicopy plasmids affect replisome positioning in *Bacillus subtilis*. J Bacteriol **186:**7084-7090.
56. **Webb, C. D., A. Teleman, S. Gordon, A. Straight, A. Belmont, D. C. Lin, A. D. Grossman, A. Wright, and R. Losick.** 1997. Bipolar localization of the replication origin regions of chromosomes in vegetative and sporulating cells of *B. subtilis*. Cell **88:**667-674.
57. **Yuan, Q., A. Carle, C. Gao, D. Sivanesan, K. A. Aly, C. Hoppner, L. Krall, N. Domke, and C. Baron.** 2005. Identification of the VirB4-VirB8-VirB5-VirB2 pilus assembly sequence of type IV secretion systems. J Biol Chem **280:**26349-26359.

609 **Table 1. *B. subtilis* strains used.**

Strain	Relevant genotype or characteristics* (reference)
CAL85	ICEBs1^{0} *str* (39)
CAL419	ICEBs1^{0} *str comK*::*cat* (39)
CAL685	*yddM*(47°)::(*lacO cat*) *thr*::(*Ppen-lacIΔ11-cfpw7 mls*) *amyE*::{(P*xyl-rapI*) *spc*}
CAL686	*yddM*(47°)::(*lacO cat*) *thr*::(*Ppen-lacIΔ11-cfpw7 mls*)
CAL688	Δ*xis190* (unmarked) *yddM*(47°)::(*lacO cat*) *thr*::(*Ppen-lacIΔ11-cfpw7 mls*) *amyE*::{(P*xyl-rapI*) *spc*}
JMA168	Δ(*rapIphrI*)*342*::*kan amyE*::{(P*spank*(*hy*)-*rapI*) *spc*} (7)
MB892	*dnaX-yfpmut2* (*tet*) *yddM*(47°)::(*lacO cat*) *thr*::(*Ppen-lacIΔ11-cfpw7 mls*)
MMB918	ICE*Bs1*::*kan lacA*::{(P*xis-yddD conE-mgfpmut2*) *tet*} *amyE*::{(P*xyl-rapI*) *spc*}
MMB919	ICE*Bs1*::*kan ydeDE*(48°)::(*lacO cat*) *thr*::(*Ppen-lacIΔ11-cfp w7 mls*)
MMB920	*dnaX-yfpmut2* (*tet*) *yddM*(47°)::(*lacO cat*) *thr*::(*Ppen-lacIΔ11-cfp w7 mls*) *amyE*::{(P*xyl-rapI*) *spc*}
MMB938	ICE*Bs1*::*kan ydeDE*(48°):(*lacO cat*) *thr*::(*Ppen-lacIΔ11-cfpw7 mls*) *amyE*::{(P*xyl-rapI*) *spc*}
MMB948	ICEBs1^{0} *cgeD*::{(P*immR-immRimmA*)*kan*} *lacA*::{(P*xis-yddD conE-mgfpmut2*) *tet*} *amyE*::{(P*xyl-rapI*) *spc*}
MMB951	Δ(*rapIphrI*)*342*::*kan* {*conEΔ*(*88-808*) (unmarked)} *amyE*::{(P*spank*(*hy*)-*rapI*) *spc*}
MMB961	Δ(*rapIphrI*)*342*::*kan* {*conEΔ*(*88-808*) (unmarked)} *lacA*::{(P*xis-yddD conE-mgfpmut2*) *tet*} *amyE*::{(P*spank*(*hy*)-*rapI*) *spc*}
MMB968	Δ(*rapIphrI*)*342*::*kan lacA*::{(P*xis-yddD conE-mgfpmut2*)*tet*} *amyE*::{(P*spank*(*hy*)-*rapI*) *spc*}
MMB973	Δ(*rapIphrI*)*342*::*kan* {*conEΔ*(*88-808*) (unmarked)} *lacA*::{(P*xis-yddD conE-mgfpmut2*)*tet*} *amyE*:: {(P*xyl-rapI*) *spc*}
MMB974	Δ(*rapIphrI*)*342*::*kan lacA*::{(P*xis-yddD conE-mgfpmut2*) *tet*} *amyE*:: {(P*xyl-rapI*) *spc*}
MMB1118	Δ(*rapIphrI*)*342*::*kan* {*conE*(*K476E*) (unmarked)} *amyE*::{(P*spank*(*hy*)-*rapI*) *spc*}
MMB1123	Δ(*rapIphrI*)*342*::*kan* {*conE*(*K476E*) (unmarked)} *thrC*::{(P*xis*-(*yddD conE-lacZ*)) *mls*} *amyE*::{(P*spank*(*hy*)-*rapI*) *spc*}
MMB1132	Δ(*rapIphrI*)*342*::*kan* {*conE*(K476E) (unmarked)} *thrC*::{(P*xis*-(*yddD-lacZ*)) *mls*} *amyE*::{(P*spank*(*hy*)-*rapI*)*spc*}
MMB1135	ICE*Bs1*::*kan lacA*::{(P*xis-yddD conE*(*K476E*)*-mgfpmut2*)*tet*} *amyE*::{(P*xyl-rapI*) *spc*}
MMB1137	ICE*Bs1*::*kan lacA*::{(P*xis-yddD conE*Δ(*88-808*)*-mgfpmut2*)*tet*} *amyE*::{(P*xyl-rapI*) *spc*}
MMB1160	Δ(*rapIphrI*)*342*::*kan* {*conE*(*K476E*) (unmarked)} *thrC*::{(P*xis*-(*conE-lacZ*)) *mls*} *amyE*::{(P*spank*(*hy*)-*rapI*) *spc*}
MMB1194	ICEBs1^{0} *str thrC*::{(P*xis*-(*yddD conE-lacZ*)) *mls*}
MMB1195	ICEBs1^{0} *str thrC*::{(P*xis*-(*conE-lacZ*)) *mls*}

610

MMB1206	Δ(*rapIphrI*)*342*::*kan* Δ*xis190* (unmarked) *lacA*::{(P*xis-yddD conE-mgfpmut2*) *tet*} *amyE*::{(P*spank*(*hy*)-*rapI*) *spc*}
MMB1218	Δ(*rapIphrI*)*342*::*kan* {*conE*(*K476E*) (unmarked)} *thrC325*::{(ICE*Bs1*-311 (Δ*attR*::*tet*)) *mls*} *amyE*::{(P*spank*(*hy*)-*rapI*) *spc*}
MMB1220	Δ(*rapIphrI*)*342*::*kan* {*conE*(*K476E*) (unmarked)} *thrC*::{(P*xis*-(*yddD conE*(*K476E*)-*lacZ*)) *mls*} *amyE*::{(P*spank*(*hy*)-*rapI*) *spc*}
MMB1245	Δ(*rapIphrI*)*342*::*kan* {*conE*(*D703A/E703A*) (unmarked)} *amyE*::{(P*spank*(*hy*)-*rapI*) *spc*}

611

612 * All strains are derived from JH642 (45) and contain *pheA1* and *trpC2*.

613

614 **Figure Legends**

615

616 **Figure 1. Genetic map of ICE*Bs1*.** *conE* (black; formerly *yddE*), regulatory genes (gray),
617 and genes required for integration, excision, and nicking (hatched) are indicated. The number of
618 transmembrane (TM) segments for each protein predicted by cPSORTdb (46) is indicated below
619 each gene. Other topology programs yield similar but not identical predictions.

620

621 **Figure 2. *conE* is required for mating of ICE*Bs1*.** Cells were grown in minimal glucose
622 medium. Mating was performed 1 hour after induction of *rapI* with 1 mM IPTG from the
623 indicated donor cells into ICE*Bs1*^{0} recipient cells (CAL419). Percent mating is the (number of
624 transconjugant CFUs per donor CFU) x 100%. The frequency reported is the average from at
625 least 2 experiments. Error bars indicate one standard deviation.

626 The asterisk (*) indicates that no transconjugants were observed. Given our limit of
627 detection, we estimate that the percent mating for these strains is $<5 \times 10^{-6}$ %.

628 Donor strains used were: a) *conE*$^+$, JMA168; b) *conE*Δ(*88-808*), MMB951; c) *conE*(*K476E*),
629 MMB1118; d) *conE*(*D703A/E704A*), MMB1245; e) *conE*(*K476E*) *thrC*::*conE*, MMB1160; f)
630 *conE*(*K476E*) *thrC*::(*yddD conE*), MMB1123; g) *conE*(*K476E*) *thrC*::*yddD*, MMB1132; h)
631 *conE*(*K476E*) *thrC*::{*yddD conE*(*K476E*)}, MMB1220; and i) *conE*(*K476E*) *thrC*::ICE*Bs1*,
632 MMB1218.

633

Figure 3. ConE-GFP localizes to the cell pole, in close association with the membrane. Cells were grown in minimal medium and samples were taken for live cell fluorescence microscopy. Cell membranes, visualized with the vital dye FM4-64, are shown in red. GFP fluorescence is artificially shown in yellow. Except for panel A, All images shown are a merge of the yellow and red. ICE*Bs1* was induced by using xylose-inducible P*xyl-rapI* (A-F) or the IPTG-inducible P*spank(hy)-rapI* (G). Cells were grown in minimal succinate and 1% xylose (A-F) was added for 2 hours prior to sampling. Cells were grown in minimal glucose with 1 mM IPTG (G) for 1 hour prior to sampling.

ConE-GFP localization in other induced ICE*Bs1*$^+$ strain backgrounds (MMB968, control for panel G; MMB974, control for panel D) was similar to that shown in panel A (data not shown). We also observed similar localization patterns for all GFP fusions in either *conE*(*Δ88-808*) or *conE*(*K476E*) donors (data not shown).

A, B. ConE-GFP in ICE*Bs1*$^+$ donor cells (MMB918).

C. ConE-GFP in *conE*(*Δ88-808*) cells (MMB973).

D. ConE(Δ88-808)-GFP in ICE*Bs1*$^+$ donor cells (MMB1135).

E. ConE-GFP in ICEBs1^0 cells (MMB948).

F. ConE(K476E)-GFP in ICE*Bs1*$^+$ donor cells (MMB1137).

G. ConE-GFP Δ*xis* donor cells (MMB1206).

654 **Figure 4. ICE*Bs1* double-stranded DNA and the replisome component Tau are more**
655 **frequently near the poles following induction of ICE*Bs1*.** Cells were grown in minimal
656 succinate media and samples were taken for live cell fluorescence microscopy. FM4-64
657 fluorescence (membrane stain) is artificially shown in gray scale. The location of *lacO* arrays
658 was visualized using LacI-CFP (cyan). The replisome subunit tau was visualized with a DnaX-
659 YFP fusion. White arrowheads indicate polar foci. Cells were grown with 1% xylose for 2 hours
660 prior to sampling. Strains contained the xylose-inducible P*xyl-rapI* (B, C, D, F).
661 A. ICE*Bs1* (*yddM*::*lacO*, *lacI-cfp*) in uninduced donor cells (CAL686).
662 B. ICE*Bs1* (*yddM*::*lacO*, *lacI-cfp*) in induced donor cells (CAL685).
663 C. 48° (*ydeDE*::*lacO*, *lacI-cfp*) in induced donor cells (MMB938).
664 D. ICE*Bs1* (*yddM*::*lacO*, *lacI-cfp*) in induced *xis*$^-$ donor cells (CAL688).
665 E. Replication protein tau (*dnaX-yfp*) in uninduced donor cells (MMB892).
666 F. Replication protein tau (*dnaX-yfp*) in induced donor cells (MMB920).
667

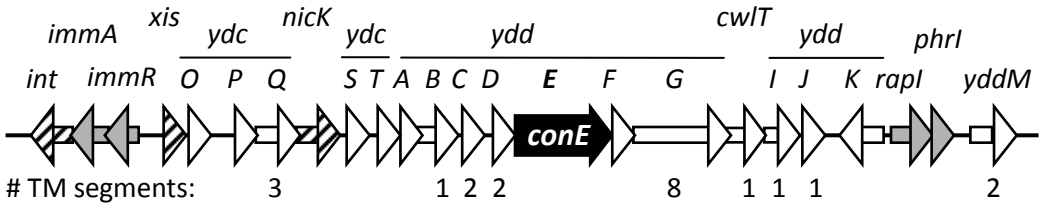
immA
xis
ydc
nicK
ydc
ydd
cwlT
ydd
phrI
int
immR
O
P
Q
S
T
A
B
C
D
E
F
G
I
J
K
rapI
yddM
conE
TM segments:
3
1
2
2
8
1
1
1
2

Figure 1

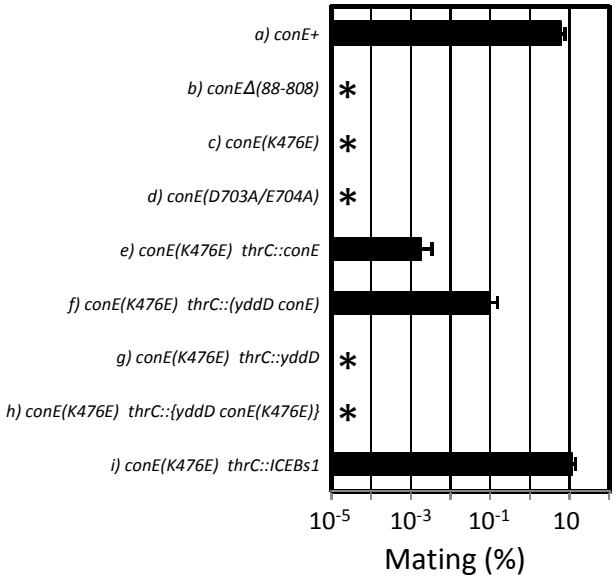
a) conE+
b) conEΔ(88-808)
c) conE(K476E)
d) conE(D703A/E704A)
e) conE(K476E) thrC::conE
f) conE(K476E) thrC::(yddD conE)
g) conE(K476E) thrC::yddD
h) conE(K476E) thrC::{yddD conE(K476E)}
i) conE(K476E) thrC::ICEBs1
*
*
*
*
*
10-5
10-3
10-1
10
Mating (%)

Figure 2

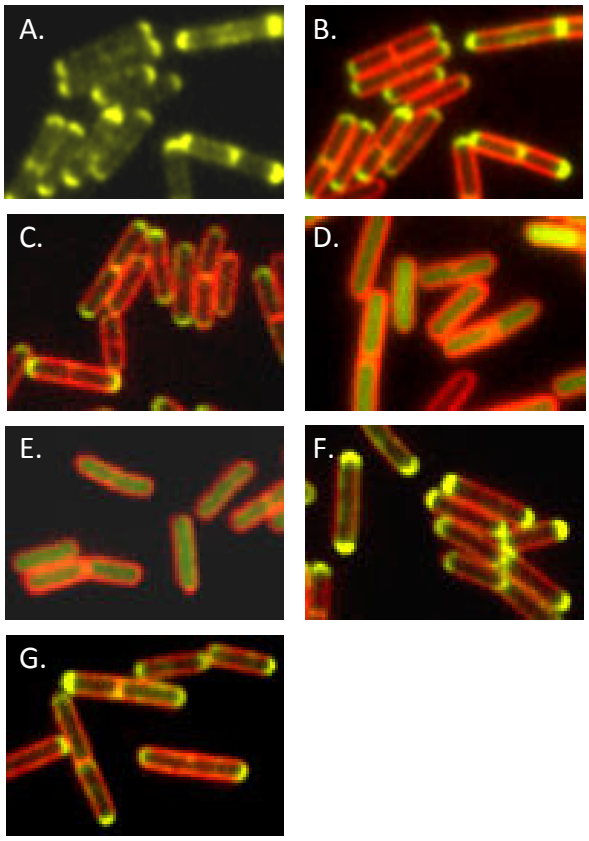

Figure 3

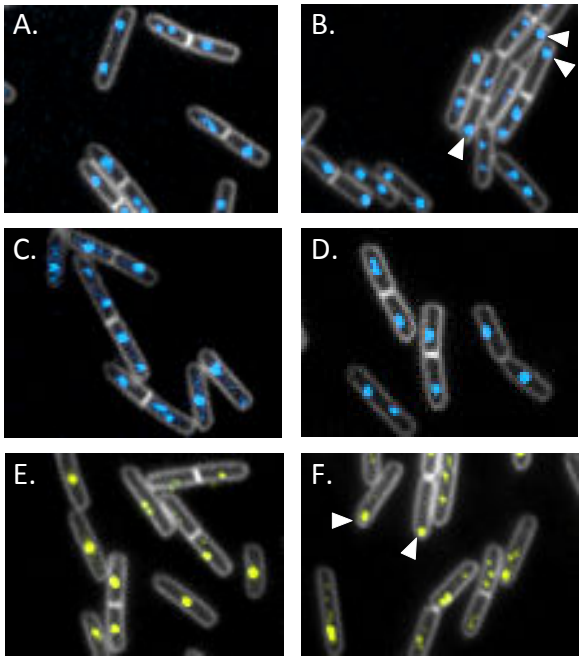

Figure 4